Fault Diagnosis of a Power Transformer Using an Improved Frequency-Response Analysis

Jong-Wook Kim, *Student Member, IEEE*, ByungKoo Park, Seung Cheol Jeong, Sang Woo Kim, *Member, IEEE*, and PooGyeon Park, *Member, IEEE*

***Abstract*—A transformer is one of the most important units in power networks; thus, fault diagnosis of transformers is quite significant. In this paper, the frequency-response analysis, deemed as a suitable diagnostic method for electrical and/or mechanical faults of a transformer, is employed to make a decision over a defective phase. To deal with wideband frequency responses of each phase, a synthetic spectral analysis is proposed, which augments low- and medium-frequency components, and equalizes the frequency intervals of a resulting combined curve by a log-frequency interpolation. Furthermore, for discriminating a defective phase through computing overall amounts of deviation with other phases, the two well-known criteria and three proposed criteria are examined with experiment data. The overall diagnosis results show that the proposed criterion discriminates a defective phase with the highest average hit ratio among all of the provided criteria for selected faults.**

***Index Terms*—Defective phase, discrimination criteria, fault diagnosis, frequency response analysis, power transformers, spectral analysis.**

I. Introduction

A high-voltage power transformer is one of the most important units in power networks; thus, the breakdown of a transformer leads to an abrupt halt of an overall process and costly repairs. To avoid this accident, monitoring systems for fault diagnosis are necessary to the power transformers in proportion to their importance.

Diagnostic methods that have been employed to the power transformers include the partial discharge (PD) method, the dissolved gas in oil analysis (DGA), and the frequency-response analysis (FRA). The PD method is applied to find the location where a partial discharge occurs by means of acoustic sensors. In this method, it is crucial how to configure the sensors and eliminate ambient noises. DGA analyzes the percentages of ingredient gases in insulating oil, and provides the relation between the obtained data and the status of a power transformer. Due to a large amount of data base accumulated during the last couple of decades, DGA has been widely used to periodically monitor power transformers. However, DGA is not suitable for detecting precise electrical and/or mechanical faults, because they affect the dissolved oil in an indirect manner. FRA generates magnitude and phase responses in frequency domains with measured input/output voltage/current signals, which are then compared with reference responses. Since electrical changes corresponding to mechanical deformations are notably observed in those frequency responses, much research has been carried out, during the last decade, on FRA [1]–[6] or the transfer function method (TFM) [7]–[11].

In FRA, the frequency responses of a test transformer are usually compared with the fingerprints of former times. However, the fingerprints are rarely available, specifically for transformers in service. Thus other information (i.e., comparison between identically constructed transformers and interphase comparison) has to be taken for diagnosis. The interphase comparison may be the last alternative, but is still a reliable method because it is based on the symmetric properties of the core-and-coil assembly [10]. It was recently reported that through the interphase comparison, any significant winding deformation is detectable with the computed deviation of a defective winding several times larger than normal deviations by the NEETRAC objective winding asymmetry (OWA) test [4], [5]. However, care must be taken to the interphase comparison because there will be differences between the FRA results owing either to differences in the lead configurations or in the winding external clearances [6]. In this paper, both the cases of with and without historical data are addressed.

Conventional FRA has been relying on a graphical analysis for diagnosis of transformers, which requires trained experts to interpret test results. To overcome this lack of objectivity, recent research employs numerical indicators such as the weighted normalized difference number [4] and the correlation coefficient [6]. Considering that the frequency responses of a power transformer retain typically ill-scaled peaks and valleys (i.e., a slight horizontal shift of a peak drastically affects a whole amount of deviation between two measurements), an appropriate indicator has to be carefully designed with justification. In this paper, qualitative analyses are made to the two general-purpose criteria and three proposed criteria considering the ill-scaled property. The proposed criteria have been sequentially designed based on the shortcomings of the former criteria. In order to verify their appropriateness, all criteria are testified by a suite of experimental data.

Manuscript received March 7, 2003; revised July 7, 2003. This work was supported in part by POSCO and in part by the Electrical and Computer Engineering Division at Pohang University of Science and Technology (POSTECH), which is funded by the Ministry of Education of Korea through its BK21 program. Paper no. TPWRD-00104-2003.

J.-W. Kim is with the Electrical Steel Sheet Research Group, Technical Research Laboratories, POSCO, Pohang 790-785, Korea (e-mail: kjune@posco.co.kr).

S. C. Jeong, S. W. Kim, and P. Park are with the Electrical and Computer Engineering Division, Pohang University of Science and Technology, Pohang 790-784, Korea (e-mail: abraham@postech.ac.kr; swkim@postech.ac.kr; ppg@postech.ac.kr).

B. Park is with the SK Teletech, Seoul 135-080, Korea (e-mail: isaac09@skteletech.co.kr).

Digital Object Identifier 10.1109/TPWRD.2004.835428

Another important factor that affects FRA performance is the quality of obtained transfer functions. As stated in [6], short-circuited turns, circulating current loops, and unground cores make changes in low-frequency responses. In addition, medium-frequency responses are sensitive to the axial movement of a winding and radial movement of the inner winding. Therefore, in order for FRA to be able to detect those faults, a synthetic spectral analysis (SSA) is proposed to generate wideband high-quality frequency responses, which augments low- and medium-frequency components by a cut-and-concatenation method (CCM). Afterwards, the resulting irregularity of the combined curve is resolved by an interpolation with respect to a logarithmic frequency scale (log-frequency interpolation hereafter), which leads to a well-balanced numerical comparison over a whole frequency range for discriminating a defective phase [4], [10].

The paper is organized as follows: Section II describes the proposed signal processing technique. Section III explains the conventional and the proposed criteria. Section IV explains detailed test setup and experiments. Section V gives the diagnostic results on simulated faults using all discrimination criteria. Section VI concludes our work and discusses future work.

II. Signal Processing Technique

In the area of system identification, parametric and nonparametric methods are provided from the parameter point of view, and the nonparametric method, which does not require the information of a model (i.e, structure, state equation and number of parameters), is more appropriate to identify such a large-scale, nonlinear, and time-varying system as a power transformer. The nonparametric method consists of transient analysis, frequency analysis, correlation analysis, and spectral analysis [12], [13]. Since frequency responses of a high quality over a wide frequency range are crucial for discriminating a defective phase, the spectral analysis is employed using the swept frequency input signal whose main advantages are better signal-to-noise ratio, wider range of frequencies, and less measuring equipment [6]. An ideal swept frequency waveform (or sweep signal) is described as

$$\begin{aligned} u(t) &= A\sin\big(2\pi g(t)t\big) \\ g(t) &= \frac{g_{\max}-g_{\min}}{t_{\rm dur}}t + g_{\min}, \quad 0 \le t \le t_{\rm dur} \end{aligned} \tag{1}$$

where A, $g_{\min}$, $g_{\max}$, and t_{dur} denote the constant gain, the prescribed minimal and maximal frequencies, and the measurement duration, respectively.

Discrete Fourier transform (DFT) in the conventional spectral analysis divides a whole frequency range with a finite number of points on a linear scale. Hence, obtained frequency responses have higher statistical weights for high than for low frequencies, which may disregard the faults relevant to the low-frequency responses. To overcome the problem, SSA is proposed to obtain the improved frequency responses where the low- and medium-frequency components are enhanced. The proposed signal processing technique includes CCM and a log-frequency interpolation which will be explained in what follows.

A. Spectral Analysis

The system model used in conventional spectral analysis is written with the convolution of input and output signals as

$$y(t) = \sum_{k=0}^{\infty} h(k)u(t-k) + v(t) \tag{2}$$

where $h(k)$, $u(t)$, $y(t)$, and $v(t)$ denote the impulse response, input, output, and noise signals, respectively. Assume that the input is a stationary stochastic process which is independent of disturbances. Replacing t with $t+\tau$, multiplying $u(t)$, and conducting expectation in both sides of (2) leads to

$$\gamma_{yu}(\tau) = \sum_{k=0}^{\infty} h(k)\gamma_u(\tau-k) \tag{3}$$

where $\gamma_{yu}(\tau) = E\{y(t+\tau)u(t)\}$ and $\gamma_u(\tau) = E\{u(t+\tau)u(t)\}$. Through DFT, the following relation for spectral densities can be derived from (3) as

$$\phi_{yu}(\omega) = H(\omega)\phi_u(\omega) \tag{4}$$

where

$$\phi_{yu}(\omega) = \frac{1}{2\pi}\sum_{\tau=-\infty}^{\infty}\gamma_{yu}(\tau)e^{-i\tau\omega} \tag{5}$$

$$\phi_u(\omega) = \frac{1}{2\pi}\sum_{\tau=-\infty}^{\infty}\gamma_u(\tau)e^{-i\tau\omega} \tag{6}$$

$$H(\omega) = \sum_{k=0}^{\infty} h(k)e^{-ik\omega}. \tag{7}$$

Now, the transfer function $H(\omega)$ can be estimated from (4) as

$$\hat{H}(\omega) = \frac{\hat{\phi}_{yu}(\omega)}{\hat{\phi}_u(\omega)} = \frac{Y_N(\omega)U_N(-\omega)}{|U_N(\omega)|^2} \tag{8}$$

where the periodograms in (8) are defined as

$$U_N(\omega) = \sum_{s=1}^{N} u(s)e^{-is\omega} \tag{9}$$

$$Y_N(\omega) = \sum_{s=1}^{N} y(s)e^{-is\omega}. \tag{10}$$

As the number of data points N tends to infinity, the variances of $\hat{\phi}_u(\omega)$ and $\hat{\phi}_{yu}(\omega)$ increase. Thus, in general, (8) produces a poor estimate of the real transfer function of a system. To overcome this deficiency, Welch's method [14] divides the input and output time series signals into overlapping sections with the number of

$$k = \left\lfloor \frac{N-n_o}{n_\omega - n_o} \right\rfloor \tag{11}$$

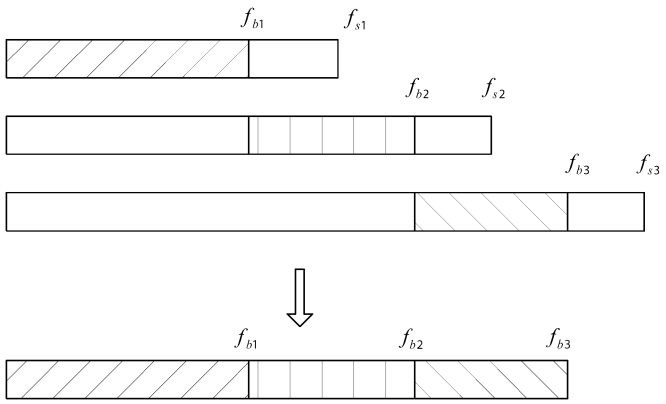

Fig. 1. Conceptional diagram of the synthesis of subfrequency responses.

where n_ω and n_o represent window length and the amount of overlap, respectively. Then, each section is filtered by a Hanning window, and its empirical transfer function is computed by (8). Finally, a smoothed but well-suited transfer function is obtained through averaging all of the temporary empirical transfer functions. Welch's method is implemented in the *spectrum function* of MATLAB, and the details are found in [15].

B. Principles of SSA

In using FRA, one should keep in mind that the sampling resolution of frequency responses affect the computation result as pointed out in [2]. A sampling resolution is calculated by

$$\Delta f = \frac{f_s}{N} \tag{12}$$

where f_s and N represent the sampling frequency and the maximum number of samples in DFT, respectively. To raise the sampling resolution, f_s should be lowered and/or N should be raised. However, to avoid the phenomenon of aliasing, sufficiently high sampling frequency is crucial to meet the Nyquist sampling theorem, which recommends f_s should be larger than the Nyquist frequency by at least two times [16]. On the other hand, if N is raised, due to the increased variance of power spectrum signals, the resulting frequency responses contain more noisy components. Thus, DFT and the spectral analysis inherently retain lower bounds of the sampling resolution. This may cause an unexpected fail to catch the meaningful information which exists in low-frequency regions of frequency responses.

To overcome this limitation, SSA based on CCM and log-frequency interpolation is proposed. Fig. 1 provides a conceptional diagram of CCM, where f_{b1}, f_{b2}, and f_{b3} denote predefined boundary frequencies, and f_{s1}, f_{s2}, f_{s3} represent the corresponding sampling frequencies. One can obtain three subfrequency responses from a set of input and output signals by only adjusting the sampling frequencies. For more reliable and informative frequency responses, separate experiments with different frequency bands of input sweep signal are recommended as in [6], which are carried out in this paper as well.

Once the subfrequency responses are obtained, three regions of interest are cut from them without overlap and concatenated into a new frequency response. If comparisons are made in separate frequency bands, the concatenation may be unnecessary. However, considering that the discrimination of a defective phase requires an overall measure of differences, a representative curve covering a whole frequency range has to be constructed by the concatenation.

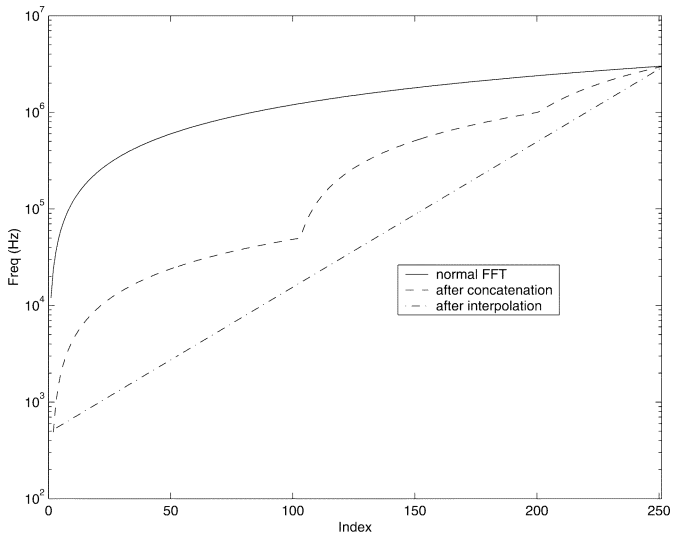

Fig. 2. Comparison of the conventional DFT and SSA results.

Thereafter, the resulting irregularity of the sampling frequencies in the combined response is corrected by the log-frequency interpolation prior to a numerical comparison. Since most significant deviations are best detected on a logarithmic scale, the interpolation process makes an amount of agreement or disagreement between the two sets of measurements quite close to what is observed with naked eyes in logarithmic frequency responses.

Fig. 2 illustrates the frequency component densities of the proposed signal processing technique against frequency indices. The solid line represents frequency components versus each index i, $1 \leq i \leq N/2$ processed by the conventional DFT with, for example, $f_s = 6$ MHz and $N = 500$. Note that low-frequency components under 100 kHz are plotted by eight points, while 166 frequency components exist above 1 MHz. Hence, the conventional DFT inevitably overemphasizes high-frequency components of frequency responses.

The dashed line in Fig. 2 plots the frequency components of a synthesized curve combined with the following boundary frequencies:

$$[\, f_{b1} \quad f_{b2} \quad f_{b3} \,] = [\, 50\,\text{kHz} \quad 1\,\text{MHz} \quad 3\,\text{MHz} \,] \tag{13}$$

which were empirically selected considering typical poles and zeros of magnitude responses. An initial frequency component of the synthesized frequency response is lowered to 500 Hz, whereas that of the conventional DFT is 10 kHz. The number of low-frequency components under 100 kHz is 108, and that of high-frequency components above 1 MHz is 50. It means that the fidelities of low- and medium-frequency components are enhanced as much by CCM.

However, the concatenated curve shows neither linear nor logarithmic increase versus frequency indices. This irregular frequency component distribution gives rise to a partially weighted measure of deviation between two frequency responses that are being compared. In order to improve the reliability of the numerical comparison, frequency components must be equally

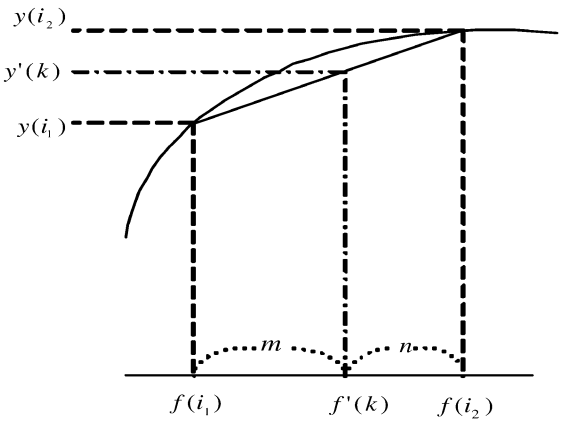

Fig. 3. Interpolation of two frequency-response points.

distributed over a whole frequency region. This can be readily implemented by a simple interpolation with a reference series where each interval is equidistant on a logarithmic scale as represented with a dash-dotted line in Fig. 2.

Fig. 3 shows the interpolation process, where $f(i_1)$ and $f(i_2)$ are two adjacent frequency components of the i_1th and i_2th indices, respectively, and $y(i_1)$ and $y(i_2)$ are the corresponding magnitude values. An interpolated magnitude value at the kth frequency component lying between $f(i_1)$ and $f(i_2)$ is approximated by the following equation:

$$\begin{aligned} y'(k) &= \frac{my(i_2)+ny(i_1)}{m+n} \\ m &= |f'(k)-f(i_1)| \\ n &= |f(i_2)-f'(k)|. \end{aligned} \tag{14}$$

An additional merit of the interpolation process is that the effect of boundary frequencies in (13) on a synthesized frequency response is minimized owing to its readjustment capability.

After the abovementioned signal processing, deviation measures are computed by a numerical criterion to discriminate a defective phase.

III. Diagnostic Criteria

In the literature of diagnosis with the artificial neural network (ANN) [17], the correlation coefficient and the standard deviation are adopted as the fingerprints of deviation between two frequency responses. However, the correlation coefficient has a serious problem under a certain condition, and the standard deviation is dominantly affected by a small number of peaks whose magnitude orders are relatively high. Thus, more proper criterion immune to such an ill-scaled property needs to be developed for further improvement. In this section, the conventional criteria and three proposed criteria are presented and investigated with qualitative analyses.

A. Sum Squared Error (SSE)

The standard deviation in [17] or the root-mean-square (rms) error in [18] can be classified as SSE

$$\delta_{\mathrm{SSE}}(x,y) = \frac{\sum_{i=1}^{N}(y_i-x_i)^2}{N} \tag{15}$$

where x_i and y_i are the ith elements of frequency responses to be compared, and N is the number of samples. When the magnitudes of x_i and y_i are of the same order for all i, SSE will compute a reasonable difference. However, if the orders of x_i and y_i differ in some region, which often occurs at peaks or valleys in magnitude responses of a power transformer, a minute horizontal shift of a peak containing no significant indication of faults will dominate SSE, while a large horizontal shift of a valley rarely affects SSE owing to its small-valued property. Therefore, the meaningful information scattered around the valley or lower values in a magnitude response is often underestimated with SSE.

B. Correlation Coefficient (CC)

CC is designed to approach 0 if the shapes of x_i and y_i are uncorrelated, and to approach 1 if their shapes are similar to each other. CC is computed by the following equation:

$$\delta_{CC}(x,y) = \frac{\sum_{i=1}^{N} x_i y_i}{\sqrt{\sum_{i=1}^{N} x_i^2 \sum_{i=1}^{N} y_i^2}} \tag{16}$$

which is normalized by the denominator terms unlike the SSE. Under a particular condition of $y_i = cx_i$ in the region $i_l \le i \le i_h$, where c is a constant, δ_{CC} equals 1 by the following reasoning:

$$\begin{aligned} \delta_{CC}(x,y) &= \frac{\sum_{i=i_l}^{i_h} x_i y_i}{\sqrt{\sum_{i=i_l}^{i_h} x_i^2 \sum_{i=i_l}^{i_h} y_i^2}} = \frac{\sum_{i=i_l}^{i_h} cx_i^2}{\sqrt{\sum_{i=i_l}^{i_h} x_i^2 \sum_{i=i_l}^{i_h} c^2 x_i^2}} \\ &= \frac{\sum_{i=i_l}^{i_h} cx_i^2}{\sqrt{\left(\sum_{i=i_l}^{i_h} cx_i^2\right)^2}} = 1, \quad i_l < i < i_h. \end{aligned}$$

This property may lead to a seriously mistaken decision. For example, assume $c = 1000$ (i.e., $y_i = 1000x_i$ for all i in a certain region). Despite such a large discrepancy between x_i and y_i, one is unaware of the deviation by CC, and subsequently fails to catch the present abnormality. Therefore, CC is considered as inadequate for the comparison of frequency responses which may include the patterns similar in shape but different in magnitude.

C. Sum Squared Ratio Error (SSRE)

SSRE is developed to normalize SSE as follows:

$$\delta_{\mathrm{SSRE}}(x,y) = \frac{\sum_{i=1}^{N}\left(\frac{y_i}{x_i-1} \to \frac{y_i}{x_i}-1\right)^2}{N} \tag{17}$$

where the ill-scaled property of SSE is ameliorated to some extent by dividing y_i with a compared response x_i. Moreover, the problem of CC is removed with SSRE as

$$\delta_{\mathrm{SSRE}}(x,y)=\frac{\sum_{i=i_l}^{i_h}\left(\frac{y_i}{x_i-1}\rightarrow\frac{y_i}{x_i}-1\right)^2}{N}=\frac{\sum_{i=i_l}^{i_h}(c-1)^2}{N}. \tag{18}$$

However, SSRE contains a defect which can be overlooked. Assume that the compared magnitude responses have the relation $y_i = k_i x_i$ and $1 \le i \le N$, where k_i is the ith ratio of the two signals. If k_i is larger than 1, the ith term in summation of (18) equals $(y_i/x_i - 1)^2 = (k_i - 1)^2$. On the contrary, if k_i is smaller than 1, $(k_i - 1)^2$ approaches 1 as k_i tends to zero. Thus, SSRE is subject to the frequency-response components of $k_i > 1$. Moreover, the position of x_i in y_i/x_i also affects the values of SSRE.

D. Sum Squared Max-Min Ratio Error (SSMMRE)

The SSMMRE is a modified version of SSRE, which is described as

$$\delta_{\mathrm{SSMMRE}}(x,y)=\frac{\sum_{i=1}^{N}\left(\frac{\max(x_i,y_i)}{\min(x_i,y_i)}-1\right)^2}{N}. \tag{19}$$

Although the aforementioned defect of SSRE is now amended, an intrinsic weakness still remains in the SSMMRE. Despite the careful signal processing techniques, a few wedge-shaped components, which contain little diagnostic information, exist in the high-frequency region of frequency responses. The effect of those meaningless components should be minimized in a well-designed criterion. To clearly illustrate the weakness of SSMMRE, consider the two compared values of $x_i = 0.0001$ and $y_i = 0.01$ (i.e., absolutely small but relatively different in terms of their orders). In this case, the term $(\max(x_i,y_i)/\min(x_i,y_i) - 1)^2$ equals 99^2, which is considerably large. Hence, the deviation of high-frequency components hard to capture with naked eyes deteriorate the objectivity of SSMMRE.

E. Absolute Sum of Logarithmic Error (ASLE)

After examining the above criteria, a more advanced criterion is proposed as

$$\delta_{\mathrm{ASLE}}(x,y)=\frac{\sum_{i=1}^{N}|20\log_{10}y_i-20\log_{10}x_i|}{N} \tag{20}$$

which is designed to realize the fully log-scaled comparison. Because ASLE is based on the comparison on a logarithmic vertical axis as shown in (20), the ill-scaled property of the SSE, the relativity problem of SSRE, and the problem at high-frequency components of SSMMRE are resolved simultaneously. Since the frequency responses have already been modified to be equidistant on a logarithmic horizontal axis, the underlying principle of ASLE is "what is seen (in spectrum analyzers) is what is calculated." This property is quite appealing because traditional approaches for fault diagnosis have been relying on the graphical information of the poles and zeros.

The phase discrimination performance of all the criteria is verified by experimental data in Section V.

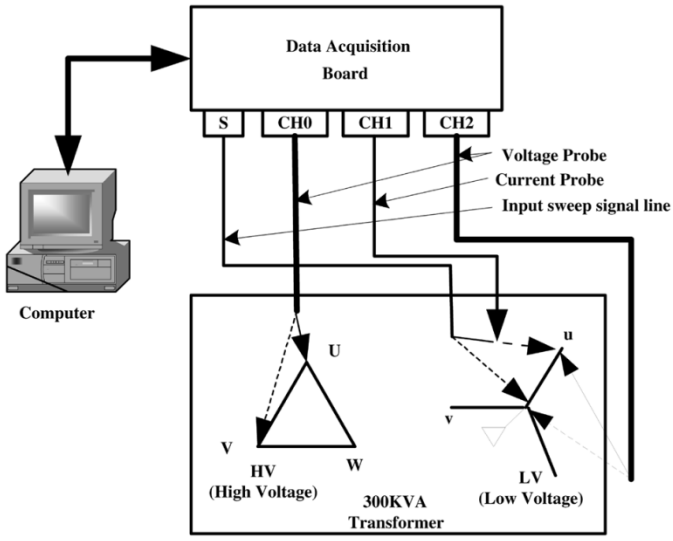

Fig. 4. Setup for the 2-MVA transformer.

TABLE I
SPECIFICATIONS OF SUBFREQUENCY BANDS

	low	medium	high
sweep freq. range	300 ~ 50KHz	50 KHz ~ 1MHz	1 ~ 3MHz
sampling freq.	500KHz	10MHz	40MHz
no. points in DFT	1024	1024	1024

IV. TEST SETUP AND EXPERIMENTS

Experimental tests are carried out on a three-phase 300-kVA 3300/440-V delta-wye transformer and a 2-MVA 3150/460-V wye-delta transformer. The instruments for data collection and typical test connections are illustrated in Fig. 4. The setup consists of an input signal generator, a data-acquisition system, a computer, and test transformers.

The Agilent 33 120 A is used as an input signal generator. Since it has insufficient output power to magnetize a transformer, an amplifying circuit including wideband operational amplifiers is implemented. By the function generator and the amplifying circuit, the input sweep signal is magnified to the range of −30–30 V and 0–4 A, and is injected to the available low-voltage bushing of the transformer during 10 ms. The whole frequency range is determined to be from 100 Hz to 3 MHz, and three subfrequency ranges for SSA are specified in Table I. Note that the sampling frequencies are ten or more times larger than upperbound frequencies in each range to meet the Nyquist theorem.

A data-acquisition system consists of four 40 Ms/s/ch (mega samples per second/ channel) analog-to-digital converters (ADCs), a main board, a current probe, and two voltage probes. The whole task of data acquisition, especially by a GPIB card and diagnostic analysis are automated on a Pentium-III 800-MHz computer.

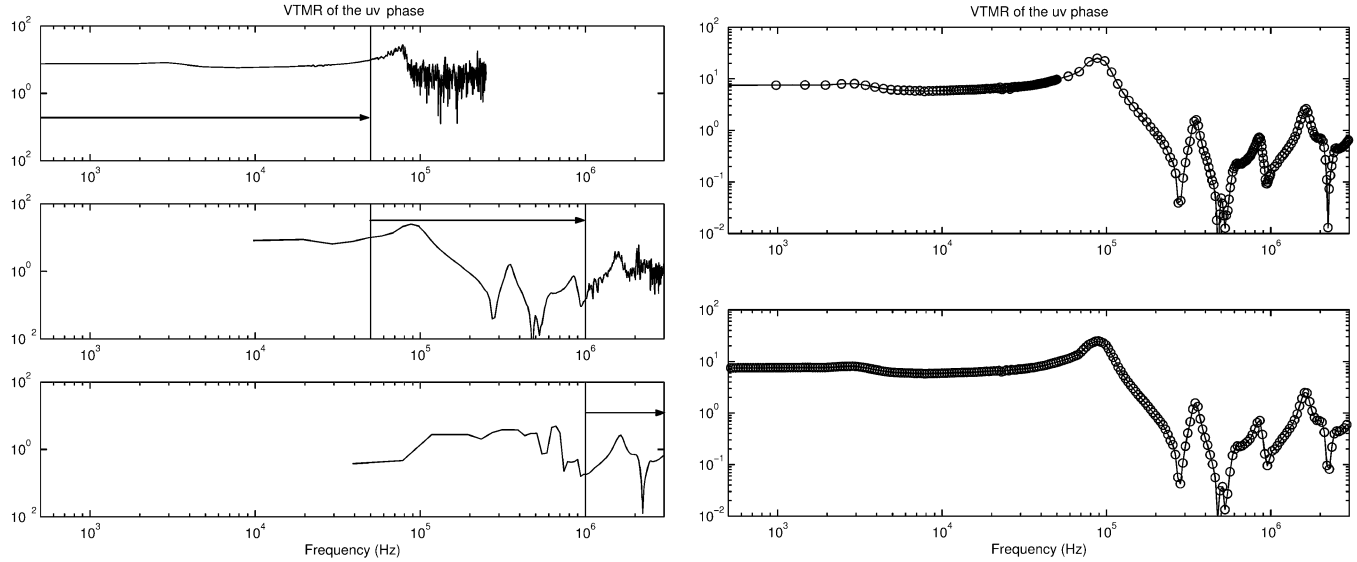

Fig. 5. Overall process of SSA. (a) Three separate subfrequency bands. (b) Log-frequency interpolation.

At a data-acquisition step, input voltage v_1, and input current i_1, of the low-voltage side are measured to estimate input impedance magnitude response (IIMR), which is calculated by replacing $u(s)$ with $i_1(s)$ in (9) and $y(s)$ with $v_1(s)$ in (10). In addition, the output voltage of a high-voltage side v_2 of the transformer is measured to estimate a voltage transfer magnitude response (VTMR), which is calculated by replacing $u(s)$ with $v_1(s)$ in (9) and $y(s)$ with $v_2(s)$ in (10). The measurements of signals i_1, v_1, and v_2 are repeated three times with changing frequency ranges of the input sweep signal as scheduled in Table I.

At a signal processing step, three sets of IIMRs and VTMRs for each subdivided frequency range are estimated by conventional spectral analysis based on (8), and they are synthesized and interpolated as described in the previous section. Since the test transformers are of a three phase type, three sets of IIMR and VTMR are estimated for each phase. Fig. 5 illustrates the overall process of SSA concerning the VTMR of the uv phase. The subplots in Fig. 5(a) represent VTMRs of the three separate subfrequency bands depicted along with arrows, which are obtained with the abovementioned specifications and cut and concatenated into a combined curve shown in the upper plot of 5 (b). The lower plot in Fig. 5(b) represents the interpolated result whose interval is constant on a logarithmic frequency scale. Note that the shape of the original magnitude response (upper plot) is preserved in the interpolated response (lower plot) except for a sharp valley at about 2 MHz. This disagreement is due to the fact that both curves are drawn with the same (250) points, and can be corrected with higher reference points for interpolation.

At a discrimination step, if reference IIMRs and VTMRs of each phase are given *a priori*, the currently obtained IIMRs and VTMRs of each phase are directly compared with them. However, considering the case of no historical data, the interphase comparison is also adopted.

The phase whose deviation is computed as the largest among three phases is determined as a defective phase in the case with

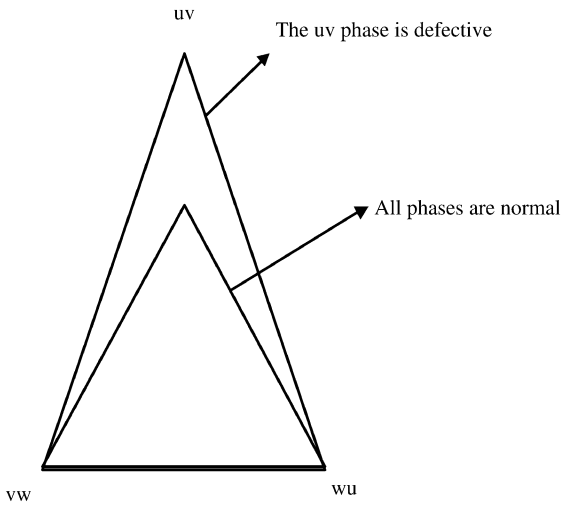

Fig. 6. Interphase comparison results when the uv phase is defective.

reference data. However, in the case of the interphase comparison, the phase excluded by two most-similar phases is the defective phase. Fig. 6 illustrates the case when the uv phase is defective, where each side length of a triangle represents the amount of deviation between two phases depicted as its terminal vertexes. Since the magnitude response of the uv phase is most different from those of the other phases, a deviation value between magnitude responses of the vw and wu phases is, conversely, the smallest among all of the pairs

$$\delta(x,y) = \begin{cases} \delta(\mathrm{MR}_{uv}, \mathrm{MR}_{vw}) \\ \delta(\mathrm{MR}_{vw}, \mathrm{MR}_{wu}) \\ \delta(\mathrm{MR}_{vw}, \mathrm{MR}_{uv}) \end{cases} \tag{21}$$

where δ denotes a measure of difference, and MR represents IIMR or VTMR of a corresponding phase. Consequently, it is a defective phase that is excluded in the phase pair computed to be most similar.

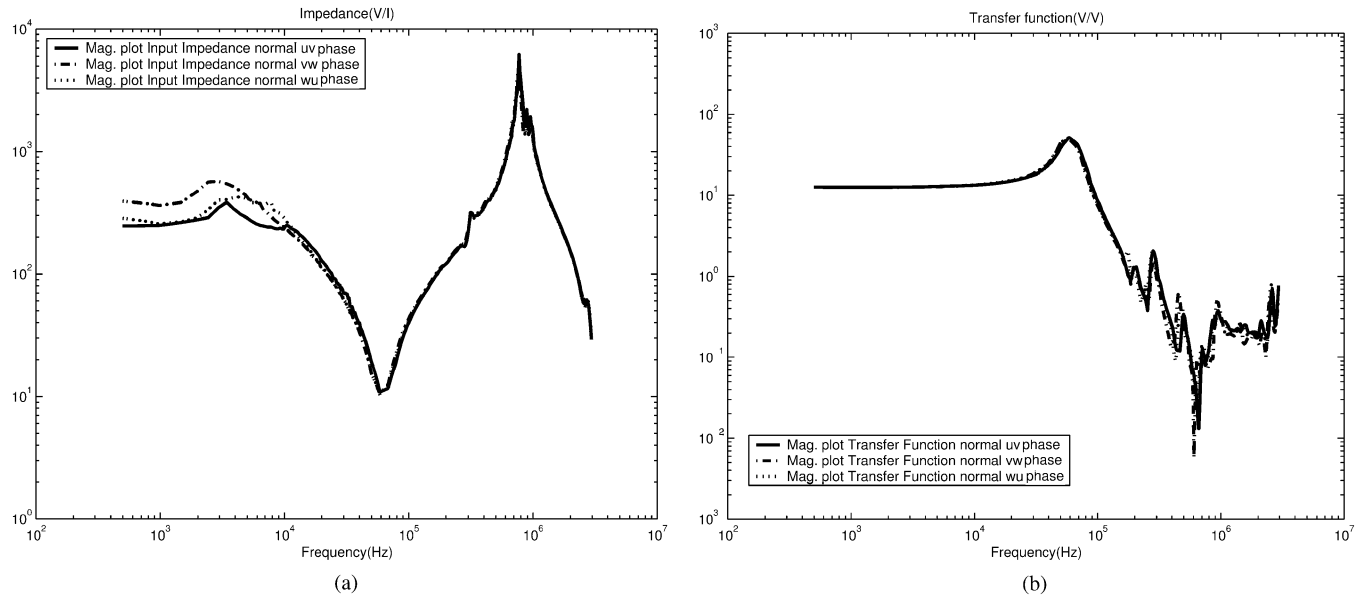

Fig. 7. Magnitude responses of a normal 300-kVA transformer. (a) Input impedance magnitude responses. (b) Voltage transfer magnitude responses.

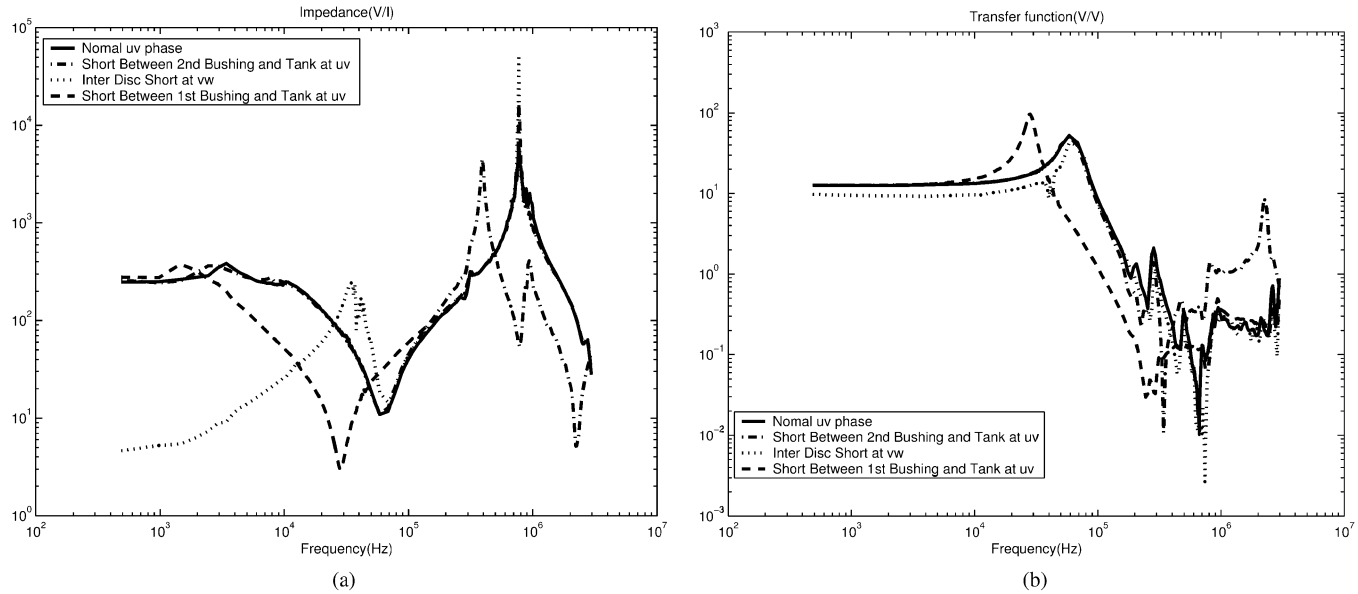

Fig. 8. Magnitude responses of various faults inflicted to a 300-kVA transformer. (a) Input impedance magnitude responses. (b) Voltage transfer magnitude responses.

V. Diagnostic Results

Artificial faults are inflicted at selected phases to simulate the faults that often occur to the transformers in service at POSCO, and are classified as

- short between HV bushing and tank (F1);
- short between LV bushing and tank (F2);
- short between tap and tank (F3);
- intertap short (F4);
- short between turn and tank (F5);
- interdisc short (F6).

IIMRs and VTMRs of a normal 300-kVA transformer are plotted in Fig. 7. The VTMR of the vw phase slightly departs from those of the other phases, because the 300-kVA transformer is particularly manufactured with seven taps drawn out from discs in this phase for the purpose of measurement. That is, the mechanical difference of the vw phase leads to an electrical change. Fig. 8 depicts several magnitude responses of artificial faults, which show apparent deviations from those of a normal phase, while the calculation of them is an another task.

The diagnostic results of two transformers are arranged in Tables II–V. Since this paper provides how to select a defective phase among three phases of power transformers (i.e., comparative method), estimating hit or miss in the phase discrimination is quite straightforward in contrast to the general fault diagnosis technique which requires threshold values between hit and miss.

TABLE II
DIAGNOSTIC RESULTS OF THE 300–kVA TRANSFORMER WITH REFERENCE DATA (O:HIT, X:MISS)

criteria	SSE		CC		SSRE		SSMMRE		ASLE	
magnitude response	II	VT	II	VT	II	VT	II	VT	II	VT
F1 at U phase	O	O	O	O	O	O	O	O	O	O
F1 at W phase	O	O	O	O	O	O	O	O	O	O
F2 at u phase	O	X	O	X	O	O	O	O	O	O
F2 at w phase	X	X	O	X	O	O	O	O	O	O
F3(tap 1) at V phase	O	O	O	O	O	O	O	O	O	O
F3(tap 7) at V phase	O	O	O	O	O	O	O	O	O	O
F4(tap 1-2) at V phase	O	X	O	X	X	O	O	O	O	O
F4(tap 6-7) at V phase	O	X	O	X	O	O	O	O	O	O
hit ratio (%)	87.5	50	100	50	87.5	100	100	100	100	100

TABLE III
DIAGNOSTIC RESULTS OF THE 2-MVA TRANSFORMER WITH REFERENCE DATA (O:HIT, X:MISS)

criteria	SSE		CC		SSRE		SSMMRE		ASLE	
magnitude response	II	VT	II	VT	II	VT	II	VT	II	VT
F1 at U phase	O	O	X	O	O	O	X	O	O	O
F2 at u phase	X	O	X	O	X	O	O	O	O	O
F5 (upper turn) at U phase	O	O	O	O	O	O	X	O	O	O
F5 (lower turn) at U phase	X	O	X	O	X	O	X	O	O	O
F6 (upper, 3%) at U phase	X	O	O	O	X	O	O	O	O	O
F6 (lower, 3%) at U phase	X	X	X	X	O	O	O	O	O	O
hit ratio (%)	33.3	83.3	33.3	83.3	50	100	50	100	100	100

In the case of having reference data, the phase whose amount of deviation from each reference data is computed as the largest is selected as a defective phase by SSE, SSRE, SSMMRE, and ASLE, while the smallest is selected as a defective phase for CC. This is due to the fact that CC is designed to yield 1 (maximum value) for normal phases, and to yield near 0 (minimum value) for defective phases. On the other hand, in the case of the interphase comparison, the phase excluded in the most similar pair (i.e., the measured difference of the pair is smallest) is determined as a defective phase by the four criteria. For instance, if the difference of the uv and vw phases is smallest, the wu phase is appointed as a defective phase as mentioned above with Fig. 6. The only difference with CC in the interphase comparison is that the most similar pair is chosen as the pair whose measured difference is nearest to 1. Then, the defective phase selected by each criterion is compared with the real defective phase where the simulated fault is inflicted. If the two phases coincide, "hit" is assigned with "O," otherwise "miss" is assigned with "X" in Tables II–V.

In Table II, the diagnostic results of the 300-kVA transformer with reference IIMRs and VTMRs for each phase are shown, where II and VT represent input impedance and voltage ratio, respectively, and U, V, and W represent the corresponding HV phases, whereas u, v, and w, are the corresponding LV phases. It is observed that if a fault occurs at the U or u phase, the IIMR and VTMR of the uv phase are the most peculiar. Similarly, in the case of a defective V or v phase, those of the vw phase deviate notably. This is straightforward if a transformer is wired as a wye-type. In a delta-type wiring, however, the u phase is an upper part in measuring the uv phase, while it is a lower part in measuring the wu phase. Thus, in terms of measurement, the fault of the u phase dominantly affects the frequency responses of the uv phase.

With reference magnitude responses, it seems simple and obvious to detect a defective phase, and even the conventional SSE can produce almost correct results as shown in Table II. Moreover, since the 300-kVA transformer is newly constructed and not used at factory sites, small faults can be readily distinguished.

Table III shows the diagnostic results of a 2-MVA transformer 30 years in service at POSCO. Unlike the 300-kVA transformer, all of the criteria with IIMRs, except the ASLE, produce hit ratios of at most 50%. At this point, it should be noted that IIMR is more reliable for the 300-kVA transformer, but VTMR is more reliable for the 2-MVA transformer. Thus, both IIMR and VTMR need to be considered at the same time for correct diagnosis. The 2-MVA transformer is considerably aged and, therefore, only an elaborate criterion such as the ASLE can distinguish the defective phases.

Tables IV and V provide diagnostic results without reference IIMRs and VTMRs of each phase. The results of a 300-kVA transformer are similar to those with reference data, but the results of a 2-MVA transformer without reference data, shown in Table V, degenerate compared with Table III. Nevertheless, the ASLE is assured to have the best discrimination capability.

The diagnostic results of two transformers are summarized in Table VI. Among various criteria, including the conventional and proposed criteria, the ASLE is thought of as the most suitable criterion via average hit ratios, in comparing such ill-scaled magnitude responses. This fact also supports our postulation that the defective phase will be best discriminated by logarithmic horizontal and vertical axes.

VI. CONCLUSION

In determining which phase has a fault in a power transformer, FRA is adopted as a basic diagnostic tool. The frequency

TABLE IV
DIAGNOSTIC RESULTS OF THE 300-kVA TRANSFORMER WITHOUT REFERENCE DATA (O:HIT, X:MISS)

criteria	SSE		CC		SSRE		SSMMRE		ASLE	
magnitude response	II	VT	II	VT	II	VT	II	VT	II	VT
F1 at U phase	O	O	O	O	O	X	O	O	O	O
F1 at W phase	X	X	O	O	O	X	O	O	O	O
F2 at u phase	O	O	O	X	O	O	O	O	O	O
F2 at w phase	O	O	O	O	O	O	O	O	O	O
F3(tap 1) at V phase	O	O	O	O	O	O	O	O	O	O
F3(tap 7) at V phase	O	O	X	O	O	O	O	O	O	O
F4(tap 1-2) at V phase	O	X	O	X	O	O	O	O	O	O
F4(tap 6-7) at V phase	O	X	O	X	O	O	O	O	O	O
hit ratio (%)	87.5	62.5	87.5	62.5	100	75	100	100	100	100

TABLE V
DIAGNOSTIC RESULTS OF THE 2-MVA TRANSFORMER WITHOUT REFERENCE DATA (O:HIT, X:MISS)

criteria	SSE		CC		SSRE		SSMMRE		ASLE	
magnitude response	II	VT	II	VT	II	VT	II	VT	II	VT
F1 at U phase	X	O	X	O	O	O	O	X	O	O
F2 at u phase	X	X	X	O	X	O	O	X	O	O
F5 (upper turn) at U phase	O	O	O	O	X	X	X	X	X	O
F5 (lower turn) at U phase	X	O	X	O	X	O	X	O	O	O
F6 (upper, 3%) at U phase	X	X	X	X	O	X	O	X	O	X
F6 (lower, 3%) at U phase	X	X	O	X	O	X	O	X	O	X
hit ratio (%)	16.7	50	33.3	66.7	50	50	66.7	16.7	83.3	66.7

TABLE VI
SUMMARY OF DIAGNOSTIC RESULTS OF THE TEST TRANSFORMERS

		SSE		CC		SSRE		SSMMRE		ASLE	
		II	VT	II	VT	II	VT	II	VT	II	VT
with reference data	300kVA (a)	87.5	50	100	50	87.5	100	100	100	100	100
	2MVA (b)	33.3	83.3	33.3	83.3	50	100	50	100	100	100
	average ($c = \frac{a+b}{2}$)	60.4	66.7	66.7	66.7	68.8	100	75	100	100	100
without reference data	300kVA (d)	87.5	62.5	87.5	62.5	100	75	100	100	100	100
	2MVA (e)	16.7	50	33.3	66.7	50	50	66.7	16.7	83.3	66.7
	average ($f = \frac{d+e}{2}$)	52.1	56.3	60.4	64.4	75	62.5	83.4	58.4	91.7	83.4
overall average hit ratio ($g = \frac{c+f}{2}$)		56.3	61.5	63.6	65.7	71.9	81.3	79.2	79.2	95.9	91.7
final hit ratio ($g' = \frac{g_1+g_2}{2}$)		58.9		64.7		76.6		79.2		93.8	

responses estimated by spectral analysis using the conventional discrete Fourier transform (DFT) have insufficient low- and medium-frequency components. To overcome the problem, SSA is proposed, which is based on CCM for high-quality frequency responses and the log-frequency interpolation for a balanced comparison over a whole frequency range.

For discriminating a defective phase, two conventional and three proposed criteria are analyzed, and benchmarks are undertaken through various experimental data. Among them, ASLE is proved to be the most pertinent criterion for selected faults via overall hit ratios. To deal with the situation of no-reference magnitude responses, three phases are compared in pairs alternatively as the interphase comparison, and even in this unfortunate case, ASLE produces satisfying results with a final hit ratio over 90%.

The fault types adopted in this paper are somewhat different from the faults for which FRA is usually employed (i.e., the faults concerning winding displacements). However, ASLE is generally designed to be the most suitable for such badly scaled responses as of transformers irrespective of fault types, unlike the blind mapping with the ANN. Therefore, we conjecture that whatever faults occur to transformers, the most deviating phase detectable by the naked eye will also be discriminated by ASLE.

In order to verify the effectiveness and scalability of the proposed method including SSA and ASLE, large power transformers up into the hundreds of megavolt-amperes, besides the kilo- and megavolt-ampere transformers, have to be tested by the proposed method for the detection of damages on large power banks and winding displacements without shorted turns.

Though the proposed method is devoted to the discrimination of a defective phase using a whole set of magnitude responses, it can also be applied to the fault diagnosis of transformers by selecting specified subfrequency bands and comparing them with corresponding fingerprints as in [6]. In addition, since historical data are usually not available in service transformers, more work has to be done on how to interpret the interphase comparison results.

ACKNOWLEDGMENT

The authors gratefully acknowledge the reviewers of this paper for their valuable advice and guidance. The authors also appreciate T. J. Park for his counterpart assistance.

REFERENCES

[1] E. P. Dick and C. C. Erven, "Transformer diagnostic testing by frequency response analysis," *IEEE Trans. Power App. Syst.*, vol. PAS-97, no. 6, pp. 2144–2153, Nov./Dec. 1978.

[2] P. T. M. Vaessen and E. Hanique, "A new frequency response analysis method for power transformer," *IEEE Trans. Power Del.*, vol. 7, no. 1, pp. 384–391, Jan. 1992.

[3] S. Birlasekaran and F. Fetherston, "Off/on-line FRA condition monitoring technique for power transformer," *IEEE Power Eng. Rev.*, pp. 54–56, Aug. 1999.

[4] L. Coffeen and J. Hildreth, "A new development in power transformer frequency response analysis to determine winding deformation WITHOUT the need for comparison to historical data [the objective winding asymmetry test]," in *Proc. EPRI Substation Equipment Diagnostics Conf. X*, San Antonio, TX, Feb. 2002.

[5] ——, "A new OBJECTIVE method for transformer frequency analysis to determine winding deformation WITHOUT the use of historical data [the objective winding asymmetry method]," in *Proc. IEEE Spring Transformers Committe Meeting*, Vancouver, BC, Canada, 2002.

[6] S. A. Ryder, "Diagnosing transformer faults using frequency response analysis," *IEEE Electr. Insul. Mag.*, vol. 19, no. 2, pp. 16–22, Mar./Apr. 2003.

[7] R. Malewski and B. Poulin, "Impulse testing of power transformers using the transfer function method," *IEEE Trans. Power Del.*, vol. 3, no. 2, pp. 476–489, Apr. 1988.

[8] S. Islam and G. Ledwich, "Locating transformer faults through sensitivity analysis of high frequency modeling using transfer function approach," in *Proc. IEEE Int. Symp. Electrical Insulation*, 1996, pp. 38–41.

[9] M. Stace and S. M. Islam, "Condition monitoring of power transformers in the Austrailian state of new South Wales using transfer function measurements," in *Proc. 5th Int. Conf. Properties and Applications of Dielectric Materials*, vol. 1, 1997, pp. 248–251.

[10] J. Christian, K. Feser, U. Sundermann, and T. Leibfried, "Diagnostics of power transformers by using the transfer function method," in *Proc. 11th Int. Symp. High Voltage Engineering*, vol. 1, 1999, pp. 37–40.

[11] N. Pinhas, S. Islam, and J. Hullett, "On the development of transfer function method for fault identification in large power transformers on load," in *Proc. Conf. Electrical Insulation and Dielectric Phenomena*, 2000, pp. 747–751.

[12] L. Ljung, *System Identification: Theory for the User*. Englewood Cliffs, NJ: Prentice-Hall, 1987.

[13] T. Söderström and P. Stoica, *System Identification*. Englewood Cliffs, NJ: Prentice-Hall, 1989.

[14] P. D. Welch, "Use of fast fourier transform for the estimation of power spectra: A method based on time averaging over short, modified periodograms," *IEEE Trans. Audio Electroacoust.*, vol. AU-15, no. 2, pp. 70–73, Jun. 1967.

[15] *Signal Processing Toolbox Users Guide*, MathWorks, Inc., Natick, MA, 1996.

[16] A. V. Oppenheim, R. W. Schafer, and J. R. Buck, *Discrete-Time Signal Processing*. Englewood Cliffs, NJ: Prentice-Hall, 1998.

[17] D. K. Xu, C. Z. Fu, and Y. M. Li, "Application of artificial neural network to the detection of the transformer winding deformation," in *Proc. High Voltage Engineering Symp.*, 1999, pp. 5.220.P5–5.223.P5.

[18] T. McKelvey, H. Akçay, and L. Ljung, "Subspace-based multivariable system identification from frequency response data," *IEEE Trans. Autom. Control*, vol. 41, no. 7, pp. 960–979, Jul. 1996.

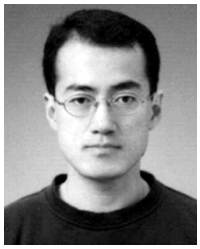

Jong-Wook Kim (S'03) was born in Youngpoong, Korea, in 1970. He received the B.S., M.S., and Ph.D. degrees from the Electrical and Computer Engineering Division at Pohang University of Science and Technology (POSTECH), Pohang, Korea, in 1998, 2000, and 2004, respectively.

Currently, he is with the Electrical Steel Sheet Research Group in Technical Research Laboratories (POSCO). His current research interests include diagnosis of electrical systems, optimization algorithm (dynamic encoding algorithm for searches), intelligent control, and system identification.

ByungKoo Park was born in Sungju, Korea, in 1975. He received the B.S. degree from the Electrical Engineering at Kyungpook National University, Taegu, Korea, in 2000 and the M.S. degree from the Electrical and Computer Engineering Division at Pohang University of Science and Technology (POSTECH), Pohang, Korea, in 2002, respectively.

Currently, he is with the R&D Center of SK Teletech, Seoul, Korea. His current research interests are the technologies concerning cellular phones, such as IS-95B, CDMA-2000, and wideband code-division multiple access (WCDMA) handsets.

Seung Cheol Jeong was born in Bosung, Korea, in 1971. He received the B.S., M.S., and Ph.D. degrees from the Electrical and Computer Engineering Division at Pohang University of Science and Technology (POSTECH) in 1997, 1999, and 2004, respectively, where he is working as a Post. Doc.

He worked on projects involving diagnosis of power transformers using the transfer function with the financial support from POSCO and the Korea Electrical Engineering and Science Research Institute. His research interests include robust and adaptive control, predictive control for constrained systems, set estimation, filter design, and diagnosis of power transformers.

Sang Woo Kim (S'83–M'91) was born in Pyungtaek, Korea, in 1961. He received the B.S., M.S., and Ph.D. degrees from the Department of Control and Instrumentation Engineering, Seoul National University, Seoul, Korea, in 1983, 1985, and 1990, respectively.

Currently, he is an Associate Professor in the Department of Electronics and Electrical Engineering at Pohang University of Science and Technology (POSTECH), Korea. He joined POSTECH in 1992 as an Assistant Professor and was a Visiting Fellow in the Department of Systems Engineering, Australian National University, Canberra, Australia, in 1993. His research interests are in optimal control, optimization algorithm, intelligent control, wireless communication, and process automation.

PooGyeon Park (M'95) was born in Korea on May 21, 1965. He received the B.S. and M.S. degrees in electrical engineering from Seoul National University, Seoul, Korea, in 1988 and 1990, respectively. He received the Ph.D. degree from Stanford University, Palo Alto, CA, in 1995.

Since 1996, he has been with the Department of Electronic and Electrical Engineering, Pohang University of Science and Technology (POSTECH), Pohang, Korea. His research interests include robust controls, predictive controls, fuzzy controls, variable structured controls, and wireless networks.